Journal of Materials & Environmental Sustainability Research (2022), 2(3): 1-11
p-ISSN: 2811-1338; e-ISSN: 2811-132X
DOI: https://doi.org/10.55455/jmesr.2022.006

Original Research Paper

Textural, thermo-gravimetric and magnetic properties of green synthesised water dispersible pristine and gold coated superparamagnetic iron oxide nanoparticles

Bamidele M. Amos-Tautua [1]*, Douye P. Markmanuel [1], Sandile P. Songca [2], Oluwatobi S. Oluwafemi [3]

[1] Department of Chemical Sciences, Niger Delta University, Wilberforce Island, Bayelsa State, Nigeria
[2] School of Chemistry and Physics, University of KwaZulu-Natal, Durban 4000, South Africa
[3] Department of Chemical Sciences, Centre for Nanomaterials, University of Johannesburg, Doornfontein 2028, Johannesburg, South Africa

*Corresponding author: Bamidele M. Amos-Tautua (bweinpere@yahoo.com)

Received: May 4, 2022; Revised: May 17, 2022; Accepted: May 17, 2022; Published: June 3, 2022

Handling Editor: Nnanake-Abasi O. Offiong

Abstract:
Gold-coated magnetic nanoparticles have received a lot of attention in recent years due to their multifunctional attributes and their prospective unique characteristics in environmental and biomedical applications. This paper reports the textural, thermo-gravimetric, and magnetic properties of green synthesized gluconic acid-capped uncoated and gold-coated superparamagnetic iron oxide nanoparticles (SPION@Au). The as-synthesized nanomaterials were characterized using scanning electron microscopy (SEM), energy-dispersive X-ray spectroscopy (EDX), thermal gravimetric analysis (TGA), Brunauer–Emmett–Teller (BET), and superconducting quantum interference device (SQUID) magnetometry. The XRD and SEM measurements showed that the gluconic acid-capped magnetic core was coated with gold with cubical spinel crystalline structures. TGA results revealed the thermal stability of the nanoparticles. Textural properties indicated that the gold-coated nanoparticles were in naturally mesoporous and exhibited the type IV isotherm with an H_2 hysteresis loop. The estimated maximum pore diameter and surface area of SPION@Au were 3.33 nm and 134.02 m^2/g respectively. Furthermore, the SQUID results showed the nanocrystals were superparamagnetic with a blocking temperature (T_B) of 214 K at 500 Oe and saturation magnetization of 11.38 emu/g. These noteworthy results demonstrated that the as-synthesized SPION@Au are promising nanomaterials for biomedical and analytical applications.

Keywords: Superparamagnetic iron oxide nanoparticles (SPION); gold coating; mesoporous; thermal stability

DOI: 10.55455/jmesr.2022.006

1. Introduction

Current developments in nanotechnology have been directed towards the establishment of superparamagnetic iron oxide nanoparticles (SPIONs), as resourceful materials for various applications in biomedicine such as targeted drug delivery (Matuszak et al. 2018; Hobson et al. 2019), magnetic resonance imaging (Usman et al., 2020; Fernández-Barahona et al., 2020), magnetic fluid hyperthermia (León Félix et al. 2019; Pardo et al. 2020), thermoablation (Kita et al. 2010), bio/immune sensing (Peng et al., 2016; Lee et al., 2020), bioseparation (Khoshneviszadeh, et al., 2020), photodynamic therapy (Fakayode et al. 2018), photothermal treatment (Nemec et al. 2020) and catalysis (Tian et al. 2011; Ferreira et al. 2020). SPIONs offer some remarkable characteristics such as high magnetic sensibility, established biocompatibility, and low toxicity which make them fit for biological and medical uses (Amos-Tautua et al. 2019a). Their distinctive tiny size and high surface area permit these nanoparticles to overcome barriers and gain entrance into biological molecules (Perni et al. 2011).

Utilizing a simple and ecologically friendly methodology for SPION synthesis is of enormous significance to enhance their biomedical applications (Dulińska-Litewka et al. 2019; Samrot et al. 2020). The green methods employed to make SPION consist of naturally occurring reagents such as ascorbic acid and plant extracts (Sood et al. 2016; Jegadeesan et al. 2019), microorganisms as reductants and capping agents, sugars and biodegradable polymers (Kharissova et al. 2013). However, the use of glucose in this work offered several unique advantages, in that glucose is readily available for use as both reducing and stabilizing agents because of its free aldehyde group. Likewise, gluconic acid, which is the oxidative product of glucose during the preparation of SPION, also functions as both dispersant and stabilizing agent for the synthesized SPION. Furthermore, glucose is cheap, mild, renewable, non-toxic, and most importantly it is eco-friendly (Lu et al. 2010). Non-toxic chemicals such as sodium borohydride, hydrazine, and dimethylformamide were used as reductants.

Pristine (uncoated) SPIONs are promising but have several disadvantages for direct use in some biomedical applications such as a high propensity to aggregate due to high surface area and magnetic dipole-dipole interaction between nanoparticles (Wu et al. 2015), rapid biodegradation when directly exposed to biological systems, and a propensity to undergo structural changes in the presence of external magnetic fields (Laurent et al. 2014). As a result, SPIONs are coated with different inert inorganic materials such as gold, silver, silica, apatite, or organic polymers like dextran, polyethyleneglycol (PEG), polyvinylacetate (PVA), and chitosan for further biomedical applications (Laurent et al. 2014). Gold has been used as the major coating material on SPION due to its favorable properties such as its low reactivity and its ability to protect the core SPION from external oxidation (Sabale et al. 2017; Ling et al. 2019; Sheel et al. 2020). Hence, SPIONs coated with Au are currently being used as potential magnetic resonance imaging contrast agents, for hyperthermia and other biological systems (Montazerabadi et al. 2015; León Félix et al. 2019; Stein et al. 2020; Yuan et al. 2022).

An elegant classification of several phases of covering iron oxide nanoparticles with gold shells is illustrated in Figure 1. From the initial contact of the gold nanoparticles which form the shell, with the iron oxide which forms the core, includes four structural types (a) iron oxide core with gold satellites; (b) continuous and discontinuous iron oxide core with continuous shells of gold and intervening silica or polymer shell; (c) other shapes of iron oxide and other materials as core with continuous shells of gold (d) variously shaped hollow structures with iron oxide nanospheres (Nguyen et al. 2018).

Green synthesis of uncoated and gold coated SPION and their characterization which include transmission electron microscopy (TEM), powder X-ray diffractometry (XRD), and ultraviolet-visible spectroscopy (UV-VIS) have been reported in our previous paper (Amos-Tautua et al. 2019). However, this paper reports the textural, thermo-gravimetric, and magnetization properties under conditions of zero-field-cooled (ZFC) and field-cooled (FC) field cooled green synthesized water-dispersible uncoated and gold-coated superparamagnetic iron oxide nanoparticles (SPION@Au).

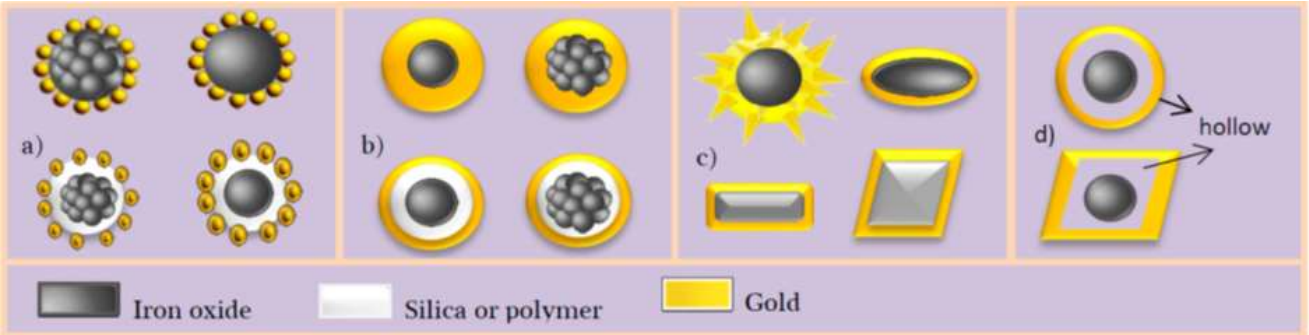

Figure 1: The different structures of core-shell nanoparticles of gold and iron oxide, based on four types (a) iron oxide core with gold satellites; (b) continuous and discontinuous iron oxide core with continuous shells of gold and intervening silica or polymer shell; (c) other shapes of iron oxide and other materials as core with continuous shells of gold (d) variously shaped hollow structures with iron oxide nanospheres. (Reproduced from Nguyen et al. (2018) under creative commons license, http://www.mdpi.org).

2. Materials and Methods

2.1 Preparation of gold-coated superparamagnetic iron- oxide nanoparticles

The synthesis of uncoated gluconic acid capped SPION has been reported in our previous work. (Amos-Tautua et al. 2020). Briefly, a solution of glucose was added to a solution of Fe (III) chloride in water to regulate the proportion of Fe (III) ion and Fe (II) ions in a 1 to 2 ratio. Then, ammonia solution (as the precipitating agent) was added to the mixture of precursors at 55 ± 2 °C to produce the superparamagnetic iron oxide nanoparticles (Amos-Tautua et al. 2020). The gold-coated SPION (SPION@Au) was prepared by reacting the as-synthesized pristine SPION with gold (III) chloride monohydrate solution at 74 °C without stirring for 4 hours (Amos-Tautua et al. 2019). The general scheme of coating gold on SPION is presented in Fig. 2(a).

2.2 Characterization

A Perkin Elmer Universal Attenuated Total Reflection UATR Spectrum Two (Buckinghamshire, UK) was used to measure the infrared spectra of the as-synthesized materials. Particle size (hydrodynamic diameter) and zeta potential were run using the Anton Paar Litesizer 500 (Graz, Austria). Scanning electron microscope (SEM, Tescan Vega 3XMU, Japan) was used to examined the surface morphology. Oxford EDX (UK) attached to SEM was used for elemental analysis. Thermo-gravimetric analysis was carried out using Hitachi STA 7200RV-TGA (Japan). Micrometrics ASAP (Accelerated Surface Area and Porosity) 2010 (USA) was used for BET porosity of the nanoparticles. The pore size distributions of SPIONs were obtained from the desorption branch of the isotherm based on the Barret-Joyner-Halenda (BJH) method. Magnetization measurements were taken at 300 K in a magnetic field (H, Oe) ranging from -20000 to 20000 Oe using the SQUID magnetometer (PPMS, Quantum Design Inc., San Diego, CA, USA). Further magnetization analysis of the SPION@gold was also achieved using a vibrating sample magnetometer, cryogenic device (UK), at the temperature range of 2–300 K at two applied magnetic fields of 100 Oe and 500 Oe.

3. Results and Discussions

3.1 Physical properties of SPION@Au

The red wine color exhibited by SPION@Au as compared to the dark brownish-black (color of a loamy soil) pristine SPION shown in Figure 2 indicates the reduction of gold chloride to gold. This process starts the deposition of colloidal particles of Au on the surface of SPION (Silva et al. 2016). Gold coating of magnetic nanoparticles is particularly fascinating since the gold surface can be further functionalized with thiol and amino groups, which permits the linkage of functional ligands such as amines and thus make the nanoparticles fit for optical and catalytic applications (Sabale et al. 2017).

Digital images in Figure 3 further illustrate the response of the as-synthesized nanoparticles under the influence of an external magnet (Figure 3(a)). On application of an external magnetic field, SPION@Au in an aqueous solution becomes magnetized up to its saturation point (b), and no residual magnetic interface was exhibited after the external magnet is withdrawn (c). The image also shows the highly dispersed SPION@Au in water (Figure 3(d)) and the clear supernatant liquid obtained when SPION@Au is drawn towards the applied external magnet (e).

3.2 FTIR studies

Figure 4 shows the FTIR studies of bare SPION and gold-coated (SPION@Au) nanomaterials. Peaks at 3314 cm^{-1} for bare SPION and 3327 cm^{-1} for SPION@Au respectively were attributed to the characteristic broad OH band of carboxylic acid. Also, the C=O peak at 1619 cm^{-1} for bare SPION shifted to 1626 cm^{-1} for SPION@Au which indicates the presence of the capping agent, gluconic acid. The bands at around 1359 and 1069 cm^{-1} are ascribed to the C–OH stretch vibration and anti-symmetric glycosidic C–O–C vibration, respectively. The existence of these peaks indicates the presence of the capping agent, gluconic acid in both nanomaterials. The stretching frequency at 564 cm^{-1} was ascribed to the Fe-O bond in SPION, but for the core-shell SPION@Au sample, the peak was moved to 570 cm^{-1}. Also, the C-O-C vibration at 1069 cm-1 was diminished and shifted to 1040 cm^{-1}. Thus, the FTIR spectra further confirmed the coating of SPION with Au (Mandal et al. 2005).

3.3Dynamic Light Scattering and Zeta potential

Dynamic light scattering measurements showed that the mean hydrodynamic diameter of SPION and SPION@Au nanoparticles were found to be 0.808 μm and 1.140 μm, respectively (Figure 5). However, the result from the electrophoretic light scattering analysis showed that both nanomaterials had a positively charged surface with a large increase in the zeta potential value from +5.6 to + 24.1 mV when the surface of SPION was coated with gold (Figure 5). The increase in both hydrodynamic size and zeta potential of SPION@Au was due to the gold coating of SPION and shows that SPION@Au was colloidally stable and dispersive, hence it could be considered for therapeutic purposes.

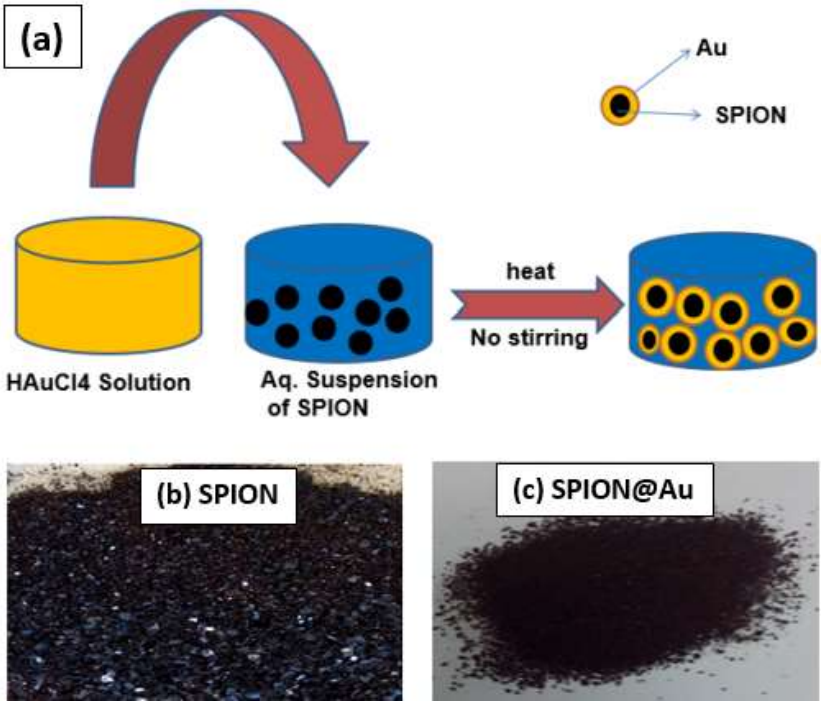

Figure 2: Schematic representation of the coating of SPION with gold (a); Digital images of SPION (b) and SPION@Au (c)

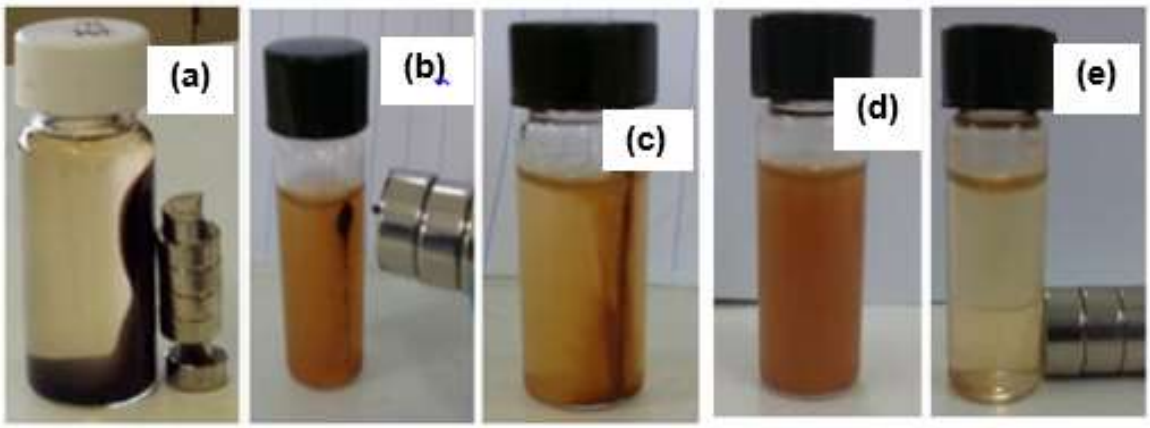

Figure 3: Digital images of the magnetic responses of SPION@Au in the presence of an external magnet. (a) magnetization of SPION@Au in an aqueous solution; (b) magnetization of SPION@Au up to saturation point; (c) SPION@Au exhibits no residual magnetization on removal of external magnet; (d) highly dispersed SPION@Au in water; (e) clear supernatant liquid obtained when SPION@Au is drawn towards the applied external magnet

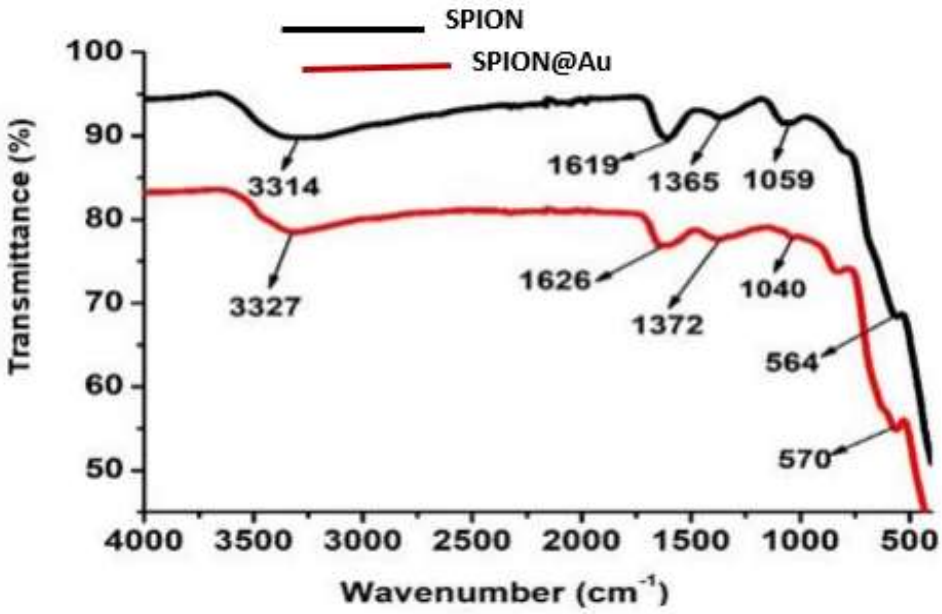

Figure 4: FTIR spectra of both SPION and SPION@Au

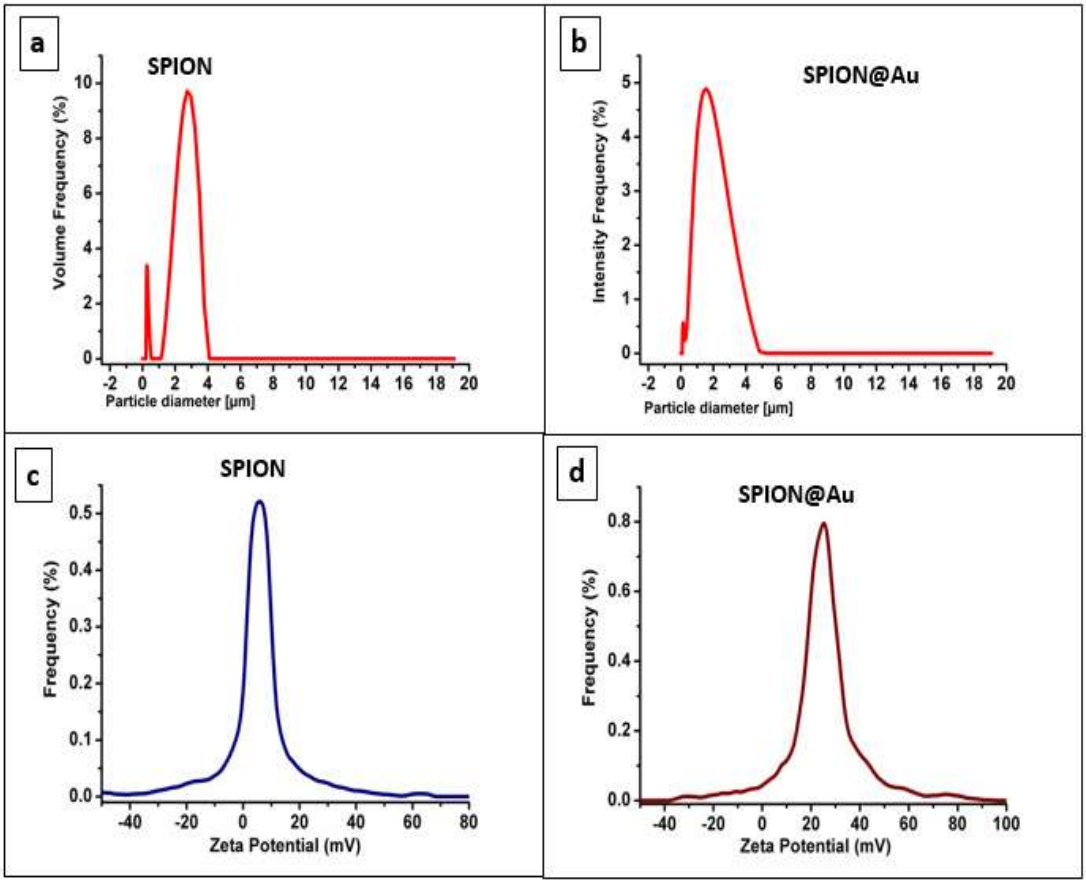

Figure 5: DLS of SPION (a), SPION@Au (b) and zeta potential of SPION (c), SPION@Au (d)

3.4 Scanning electron microscopy (SEM)

The SEM images of SPION and SPION@Au are shown in Figure 6 for comparison. The SEM image of uncoated SPION shows a highly monodispersed mixture exhibiting isometric face-centered cubic (fcc) octahedral geometry with a mixture of small and large-sized particles (Figure 6a), while in the image of SPION@Au (Figure 6c), the iron oxide particles have more cluster-like compositions. In addition, the SEM image of SPION@Au (Figure 6c) revealed the presence of gold as colloidal particles deposited on the surface of the magnetic iron oxides core. Therefore, the system may be classified according to Nguyen et al. (2018) as having iron oxide cores with gold satellites. The EDX spectra of both samples show the presence of C, Fe and O (Figures 6 b and d). In addition, the EDX of SPION@Au showed the presence of Au (figure 6d) which confirmed that gold was actually deposited on the core of SPION.

3.5Thermo-gravimetric analysis

The thermogravimetric analysis/derivative thermogravimetric (TGA/DTG) curves of SPION and SPION@Au are shown in Figure 7. The DTG curve of SPION@Au shows five main derivative peaks at 106 °C, 259 °C, 382 °C, 481 °C, and 808 °C as compared to four at 142 °C, 253 °C, 426 °C, and 840 °C for SPION. The initial weight loss of 5% in the temperature range of 27 – 106 °C of SPION@Au was due to water absorbed into the nanoparticles. Maximum degradation of the capped gluconic acid of SPION@Au which accounted for 15% weight loss took place in the range of 106 – 481 °C. The presence of a smooth horizontal section in the curves for both SPION and SPION@Au above 800 °C showed the complete transformation of the nanomaterials into magnetic iron oxides nanoparticles and confirmed their thermal stability. The residual mass of SPION@Au obtained was 78%. Comparing the TG analysis of both SPION and SPION@Au, more water (9%) and organic matter (19%) were lost from the pristine SPION than from the SPION@Au sample. Also, 78% of the SPION@Au was left as a residue after the thermal degradation relative to 69% of iron oxide that remained after the thermal decomposition of SPION. These results confirmed the thermal stability presence of SPION@Au.

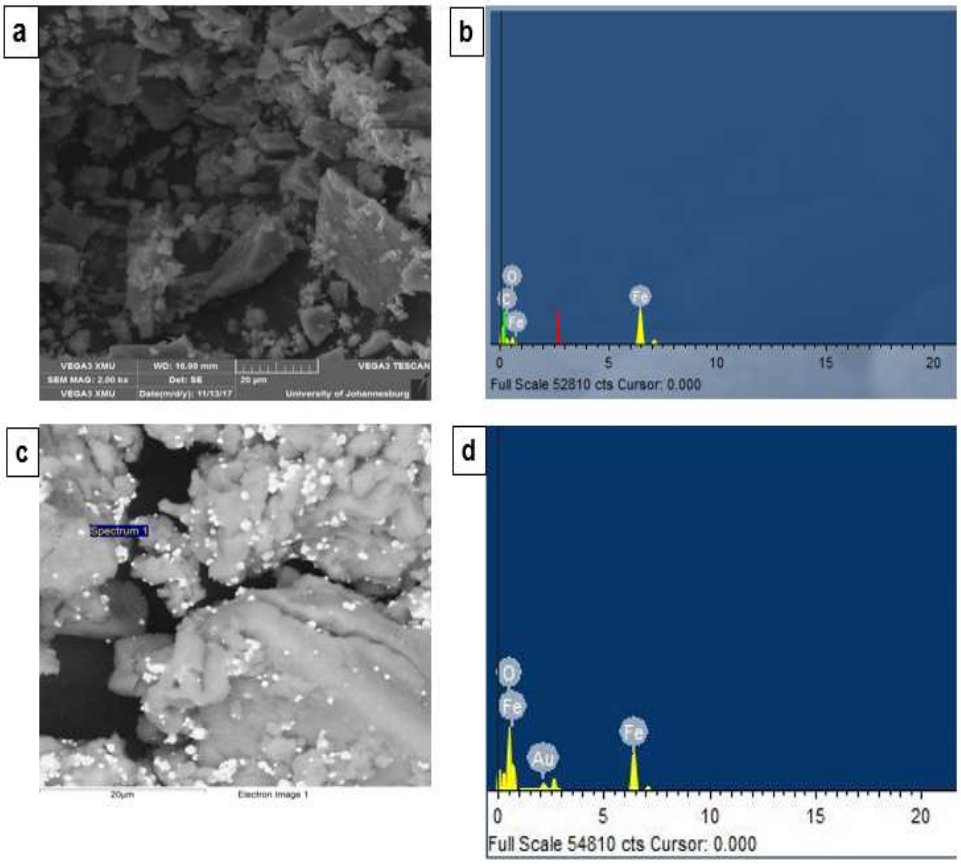

Figure 6: SEM images of SPION (a); EDX spectra of SPION (b); SEM of SPION@Au (c) and EDX of SPION@Au (d)

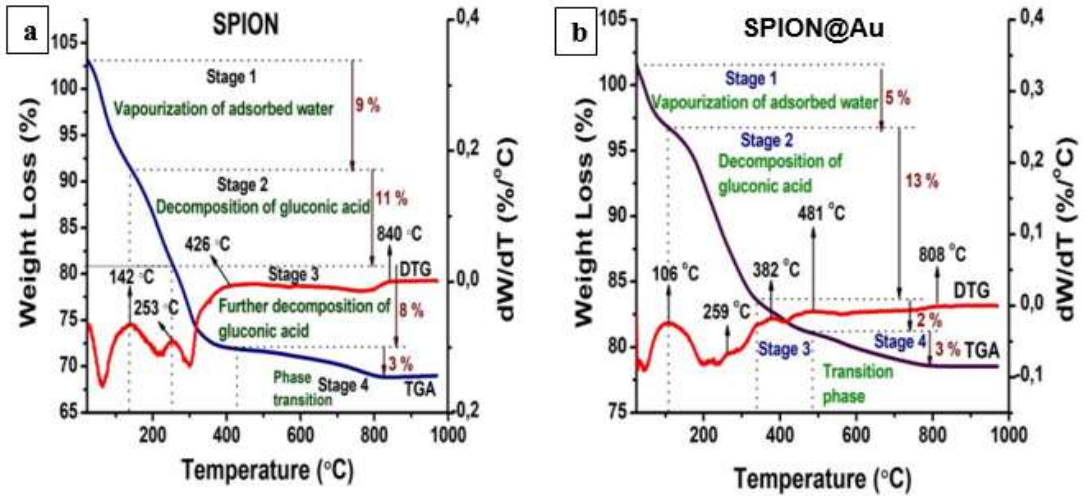

Figure 7: TGA/DTG curves of SPION and SPION@Au

3.6 Textural properties

Further characterization was carried out by comparing the surface area and porosity of SPION and SPION@Au as determined by the BET method. The N_2 physisorption curves of both samples (Figure 8) showed that they exhibited the H_2 hysteresis loop and Type IV isotherm that are related to capillary condensation in mesopore structures. It could also be deduced from the hysteresis nature that the nanoparticles contain ink bottle-like pores. However, the hysteresis loop of SPION@Au was broader than that of SPION which can be ascribed to the covering of the pristine SPION with Au. The estimated surface area and maximum pore diameter of SPION@Au were 134.02 m^2/g and 3.33 nm respectively which are slightly lower than those of SPION with the surface area and pore diameter of 165.56 m^2/g and 3.37 nm respectively. These noteworthy textural properties of the as-synthesized nanoparticles could play a significant role in physisorption and in environmental remediation of heavy metals pollution (Amos-Tautua et al. 2020; Getahun et al. 2022).

Magnetization (Ms) values measured at 300 K (Figure 9) for the magnetic core SPION (11.17 emu/g) and the gold-coated SPION@Au (11.38 emu/g) are almost the same. This shows that the superparamagnetic fraction of the SPION was retained by the coating of its surface with gold which agrees with literature reports that passivation of SPION surfaces with Au had a negligible decrease in their magnetic performance (Sun et al. 2007; Wu et al. 2015). To further explain the magnetic state of SPION@Au, magnetization curves in conditions of zero-field-cooled (ZFC) and field-cooled (FC) curves were obtained as shown in Figure 9. Measurements were performed in the temperature range of 2–300 K, at two applied magnetic fields of 100 Oe and 500 Oe. Differences in the magnetization of SPION@Au in the ZFC and FC modes shows its superparamagnetic performance (Chesnel et al. 2014).

The blocking temperature (TB) of the gold-coated SPION nanocrystals was also determined at the two applied fields of 100 Oe and 500 Oe. TB shows the transformation involving the superparamagnetic condition and blocked status and is typically related to the maximum in the ZFC curve, where the thermal energy is almost similar to the anisotropy energy barrier (Caruntu et al. 2007). Subsequently, the estimated TB for SPION@Au was 214 K at 500 Oe. Conversely, no maximum was observed in the ZFC curve at 100 Oe, hence it is assumed that the TB of the largest nanoparticles is located above 300 K at 100 Oe magnetic field. However, a shoulder in the ZFC curves for both 100 Oe and 500 Oe can be observed at low temperatures ~22 K and ~56 K, respectively. This may imply that the temperature dependence of the magnetic response did not affect the dipole-dipole interactions of SPION@Au nanoparticles (López-Cruz et al. 2009). Again, the shape of the FC curve at 500 Oe (different from that of 100 Oe) may be as a result of dipole-dipole linkages between the gold-coated iron-oxide nanoparticles which are plausibly associated with the formation of more aggregates of SPION@Au as observed in both SEM (Figure 6) (del Barco et al. 2001; Suber et al. 2005). These magnetic properties imply the promising use of SPION@Au for biomedical applications such as magnetic hyperthermia, and delivery of photosensitizers in photodynamic therapy and could be used as a magnetic resonance imaging contrasting agent.

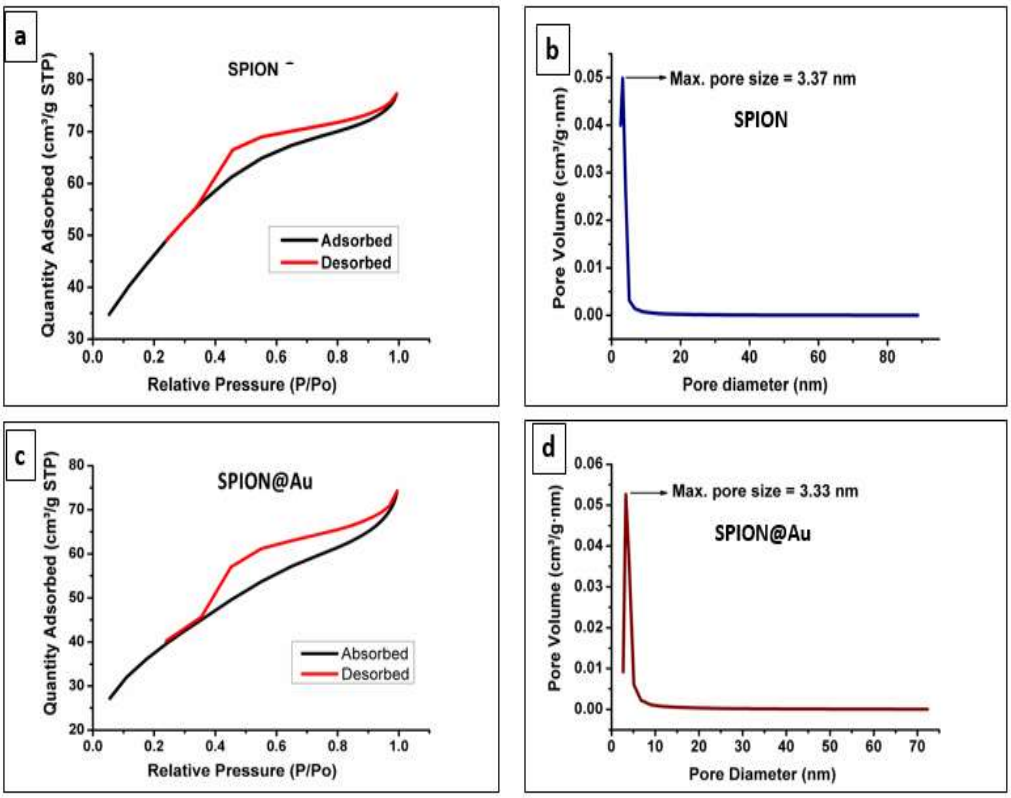

Figure 8: Nitrogen adsorption-desorption isotherms of SPION (a); SPION@Au (c); and pore size distribution of SPION (b) and SPION@Au (d)

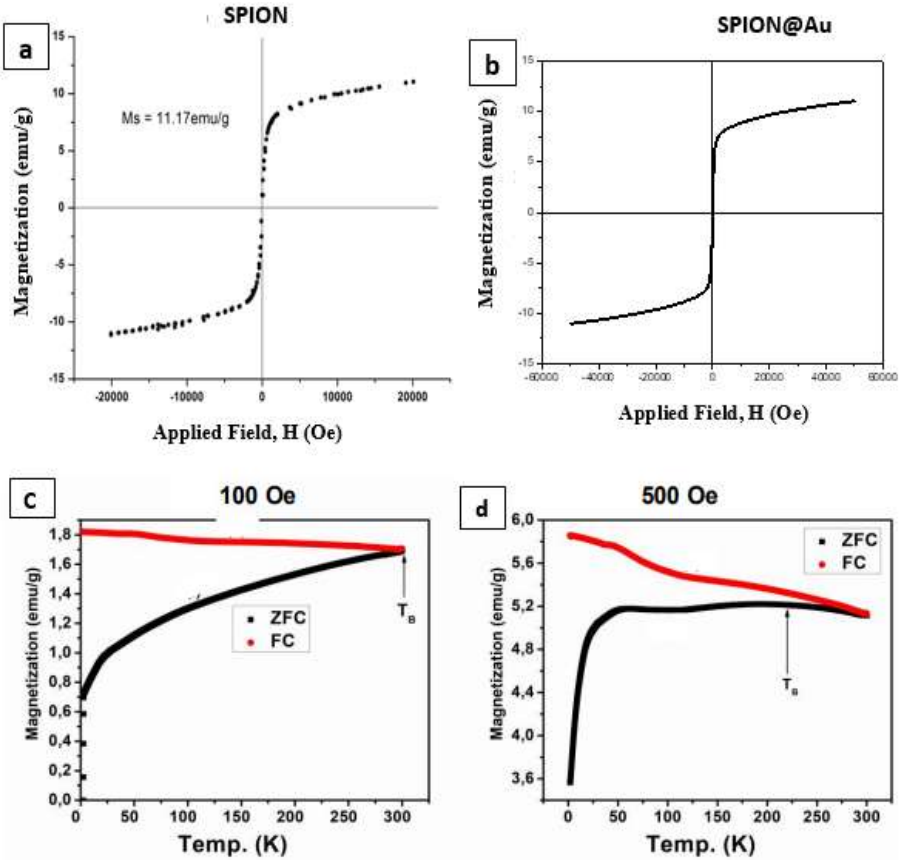

Figure 9: Magnetization curves of (a) SPION at 300K; (b) SPION@Au at 300K; VSM analysis of SPION@Au (c) Zero field cooling and field cooling at 100 Oe; (d) SPION@Au zero field cooling and field cooling at 500 Oe

4. Conclusion

Pristine (uncoated) and gold-coated gluconic acid-capped superparamagnetic iron oxide nanoparticles were characterized using both spectroscopic and microscopic methods. Iron oxide nanoparticles were clearly shown by SEM with gold satellites deposited on their surface. The as-synthesized nanocrystals are thermally stable and exhibited high surface area and moderate magnetic susceptibility hence they could be considered good materials for storage, catalysis, sensors, physisorption, and biomedical applications.

Authors contribution

Conceptualization, BMA-T, SPS, and OSO; methodology, BMA-T; writing—original draft preparation, BMA-T; writing—review and editing, DPM and SPS; supervision, OSOS, and SPS; funding acquisition, SPS and OSO.

Conflict of interests

No conflict of interest is declared by the authors concerning this work.

Funding

This work was funded by National Research Foundation (NRF), South Africa under the Nanotechnology Flagship Programme (Grant no: 97983 and 107619) and DST/NRF Collaborative Postgraduate Training program (Grant no: 92553 and 105262), and carried out at the University of Johannesburg, South Africa.

References

Amos-Tautua, B. M., Fakayode, O. J., van Vuuren, S., Songca, S. P. & Oluwafemi, O. S. (2019). Non distorted visible light-absorbing thiol-PEGylated gold-coated superparamagnetic iron oxide nanoparticles–porphyrin conjugates and their inhibitory effects against nosocomial pathogens. *MRS Communications*, 9(4), 1335-1342.

Amos-Tautua, B. M., Fakayode, O. J., Songca, S. P. & Oluwafemi, O. S. (2020). Effect of synthetic conditions on the crystallinity, porosity and magnetic properties of gluconic acid capped iron oxide nanoparticles. *Nano-Structures & Nano-Objects*, 23, 100480.

Caruntu, D., Caruntu, G. & O'Connor, C. J. (2007). Magnetic properties of variable-sized Fe_3O_4 nanoparticles synthesized from non-aqueous homogeneous solutions of polyols. *Journal of Physics D: Applied Physics*, 40(19), 5801.

Chesnel, K., Trevino, M., Cai, Y., Hancock, J.M., Smith, S.J. & Harrison, R.G. (2014). Particle size effects on the magnetic behaviour of 5 to 11 nm Fe_3O_4 nanoparticles coated with oleic acid. *Journal of Physics: Conference Series*, 521(1), 1-3, Article ID 012004.

del Barco, E., Asenjo, J., Zhang, X.X., Pieczynski, R., Julia, A., Tejada, J., Ziolo, R.F., Fiorani, D. & Testa, A.M. (2001). Free rotation of magnetic nanoparticles in a solid matrix. *Chemistry of Materials*, 13(5), 1487-1490.

Dulińska-Litewka, J., Łazarczyk, A., Hałubiec, P., Szafrański, O., Karnas, K. & Karewicz, A. (2019). Superparamagnetic iron oxide nanoparticles—Current and prospective medical applications. *Materials*, 12(4), 617. DOI: 10.3390/ma12040617

Fakayode, O. J., Tsolekile, N., Songca, S. P. & Oluwafemi, O. S. (2018). Applications of functionalized nanomaterials in photodynamic therapy. *Biophysical Reviews*, 10(1), 49-67.

Fernández-Barahona, I., Muñoz-Hernando, M., Ruiz-Cabello, J., Herranz, F., and Pellico, J. (2020). Iron oxide nanoparticles: an alternative for positive contrast in magnetic resonance imaging. *Inorganics*, 8 (4), 28. DOI: 10.3390/inorganics8040028

Ferreira, L. F. P., de Oliveira, T. M., Toma, S. H., Toyama, M. M., Araki, K. & Avanzi, L. H. (2020). Superparamagnetic iron oxide nanoparticles (SPIONs) conjugated with lipase *Candida antarctica A* for biodiesel synthesis. *RSC Advances*, 10(63), 38490-38496.

Getahun, Y., Gardea-Torresdey, J., Manciu, F. S., Li, X. & El-Gendy, A. A. (2022). Green synthesized superparamagnetic iron oxide nanoparticles for water treatment with alternative recyclability. *Journal of Molecular Liquids*, *356*, 118983. DOI: 10.1016/j.molliq.2022.118983

Hobson, N. J., Weng, X., Siow, B., Veiga, C., Ashford, M., Thanh, N. T., Schätzlein, A.G. & Uchegbu, I. F. (2019). Clustering superparamagnetic iron oxide nanoparticles produces organ-targeted high-contrast magnetic resonance images. *Nanomedicine*, 14(9), 1135-1152.

Jegadeesan, G. B., Srimathi, K., Srinivas, N. S., Manishkanna, S. & Vignesh, D. (2019). Green synthesis of iron oxide nanoparticles using Terminalia bellirica and Moringa oleifera fruit and leaf extracts: antioxidant, antibacterial and thermoacoustic properties. *Biocatalysis and Agricultural Biotechnology*, 21, 101354. DOI: 10.1016/j.bcab.2019.101354

Kharissova, O.V., Dias, H.V.R., Kharisov, B.I., Perez, B.O., Perez, V.M.J. (2013). The greener synthesis of nanoparticles. *Trends in Biotechnology*, 31, 240- 248.

Khoshneviszadeh, M., Zargarnezhad, S., Ghasemi, Y. & Gholami, A. (2020). Evaluation of surface-modified superparamagnetic iron oxide nanoparticles to optimize bacterial immobilization for bio-separation with the least inhibitory effect on microorganism activity. *Nanoscience & Nanotechnology-Asia*, 10(2), 166-174.

Kita, E., Oda, T., Kayano, T., Sato, S., Minagawa, M., Yanagihara, H., Kishimoto, M., Mitsumata, C., Hashimoto, S., Yamada, K. & Ohkohchi, N. (2010). Ferromagnetic nanoparticles for magnetic hyperthermia and thermoablation therapy. *Journal of Physics D: Applied Physics*, 43, 474011-22.

Laurent, S., Saei, A.A., Behzadi, S., Panahifar, A. & Mahmoudi, M. (2014). Superparamagnetic iron oxide nanoparticles for delivery of therapeutic agents: opportunities and challenges. *Expert Opinion in Drug Delivery*, 11(9), 1449–1470

Lee, C. N., Chiu, L. H., Fang, C. L., Yeh, S. D., Zuo, C. S., Chen, S. C., Kuo, L.K., Wang, Y.M. & Lai, W. F. T. (2020). Synthesis, characterization, and application of superparamagnetic iron oxide nanoprobes for extra-pulmonary tuberculosis detection. *Journal of Visualized Experiments*, (156), e58227. DOI: 10.3791/58227

León Félix, L., Sanz, B., Sebastián, V., Torres, T. E., Sousa, M. H., Coaquira, J. A. H., Ibarra, M.R. & Goya, G. F. (2019). Gold-decorated magnetic nanoparticles design for hyperthermia applications and as a potential platform for their surface-functionalization. *Scientific Reports*, 9(1), 1-11.

Ling, W., Wang, M., Xiong, C., Xie, D., Chen, Q., Chu, X., Qiu, X., Li, Y. & Xiao, X. (2019). Synthesis, surface modification, and applications of magnetic iron oxide nanoparticles. *Journal of Materials Research*, 34(11), 1828-1844. DOI: 10.1557/jmr.2019.129

López-Cruz, A., Barrera, C., Calero-DdelC, V.L. & Rinaldi, C. (2009). Water dispersible iron oxide nanoparticles coated with covalently linked chitosan. *Journal of Materials Chemistry*, 19(37), 6870-6876.

Lu, W., Shen, Y., Xie, A. & Zhang, W. J. (2010). Green synthesis and characterization of superparamagnetic Fe3O4 nanoparticles. *Journal of Magnetism & Magnetic Materials*, 322, 1828-1833.

Mandal, M., Kundu, S., Ghosh, S.K., Panigrahi, S., Sau, T.K., Yusuf, S.M. and Pal, T. (2005). Magnetite nanoparticles with tunable gold or silver shell. *Journal of Colloid and Interface Science*, 286(1), 187-194.

Matuszak, J., Lutz, B., Sekita, A., Zaloga, J., Alexiou, C., Lyer, S., & Cicha, I. (2018). Drug delivery to atherosclerotic plaques using superparamagnetic iron oxide nanoparticles. International Journal of Nanomedicine, 13, 8443.

Montazerabadi, A. R., Oghabian, M. A., Irajirad, R., Muhammadnejad, S., Ahmadvand, D., Delavari H, H. & Mahdavi, S. R. (2015). Development of gold-coated magnetic nanoparticles as a potential MRI contrast agent. *Nano*, 10(04), 1550048.

Nemec, S., Kralj, S., Wilhelm, C., Abou-Hassan, A., Rols, M. P. & Kolosnjaj-Tabi, J. (2020). Comparison of iron oxide nanoparticles in photothermia and magnetic hyperthermia: Effects of clustering and silica encapsulation on nanoparticles' heating yield. *Applied Sciences*, 10(20), 7322.

Nguyen, T.T., Mammeri, F., Ammar, S. (2018). Iron oxide and gold based magneto-plasmonic nanostructures for medical applications: a review. *Nanomaterials*, 8(3): 149.

Pardo, A., Pelaz, B., Gallo, J., Banobre-Lopez, M., Parak, W. J., Barbosa, S., del Pino, P. & Taboada, P. (2020). Synthesis, characterization, and evaluation of superparamagnetic doped ferrites as potential therapeutic nanotools. *Chemistry of Materials*, 32(6), 2220-2231.

Peng, D., Liang, R.-P., Huang, H., & J.-D. Qiu, J.-D. (2016). Electrochemical immunosensor for carcinoembryonic antigen based on signal amplification strategy of graphene and Fe_3O_4/Au NPs. *Journal of Electroanalytical Chemistry*, 761, 112–117.

Perni, S., Prokopovich, P., Pratten, J., Parkin, I. P. & Wilsona, M. (2011). Nanoparticles: their potential use in antibacterial photodynamic therapy. *Photochemistry & Photobiological Sciences*, 10, 712-720.

Sabale, S., Kandesar, P., Jadhav V., Komorek R., Motkuri, R.K. & Yu, X-Y. (2017). Recent developments in the synthesis, properties, and biomedical applications of core/shell superparamagnetic iron oxide nanoparticles with gold. *Biomaterial Science*, 5, 2212–2225.

Samrot, A. V., Sahithya, C. S., Selvarani, J., Purayil, S. K. & Ponnaiah, P. (2021). A review on synthesis, characterization and potential biological applications of superparamagnetic iron oxide nanoparticles. *Current Research in Green and Sustainable Chemistry*, 4, 100042. DOI: 10.1016/j.crgsc.2020.100042

Sheel, R., Kumari, P., Panda, P. K., Ansari, M. D. J., Patel, P., Singh, S., Kumari, B., Sarkar, B., Mallick, M.A.& Verma, S. K. (2020). Molecular intrinsic proximal interaction infer oxidative stress and apoptosis modulated *in vivo* biocompatibility of *P. niruri* contrived antibacterial iron oxide nanoparticles with zebra fish. *Environmental Pollution*, 267, 115482. DOI: 10.1016/j.envpol.2020.115482

Silva, A.H., Lima, E., Mansilla, M.V., Zysler, R.D., Troiani, H., Pisciotti, M.L.M., Locatelli, C., Benech, J.C., Oddone, N., Zoldan, V.C., Winter, E., Pasa, A.A. & Creczynski-Pasa, T.B. (2016). Superparamagnetic iron-oxide nanoparticles mPEG350- and mPEG2000-coated: Cell uptake and biocompatibility evaluation. *Nanomedicine: Nanotechnology, Biology, and Medicine*, 12(4), 909–919.

Sood, A., Arora, V., Shah, J., Kotnala, R. K. & Jain, T. K. (2016). Ascorbic acid-mediated synthesis and characterisation of iron oxide/gold core–shell nanoparticles. *Journal of Experimental Nanoscience*, 11(5), 370-38.

Stein, R., Friedrich, B., Mühlberger, M., Cebulla, N., Schreiber, E., Tietze, R., Cicha, I., Alexiou, C., Dutz, S., Boccaccini, A.R.& Unterweger, H. (2020). Synthesis and characterization of citrate-stabilized gold-coated superparamagnetic iron oxide nanoparticles for biomedical applications. *Molecules*, 25(19), 4425.

Suber, L., Imperatori, P., Ausanio, G., Fabbri, F. & Hofmeister, H. (2005). Synthesis, morphology, and magnetic characterization of iron oxide nanowires and nanotubes. *The Journal of Physical Chemistry B*, 109(15), 7103-7109.

Sun, Q., Reddy, B.V., Marquez, M., Jena, P., Gonzalez, C. & Wang, Q. (2007). Theoretical study on gold-coated iron oxide nanostructure: Magnetism and bioselectivity for amino acids. *The Journal of Physical Chemistry C*, 111(11), 4159-4163.

Tian, Y., Wu, D., Jia, X., Yu, B. & Zhan, S. (2011). Core-shell nanostructure of α-Fe2O3/Fe3O4: Synthesis and photocatalysis for methyl orange. *Journal of Nanomaterials*, 2011, (29), 1-4.

Usman, A., Patterson, A. J., Yuan, J., Cluroe, A., Patterson, I., Graves, M. J., Gillard, J.H. & Sadat, U. (2020). Ferumoxytol-enhanced three-dimensional magnetic resonance imaging of carotid atheroma-a feasibility and temporal dependence study. *Scientific Reports*, 10(1), 1-15.

Wu, W., Wu, Z., Yu, T., Jiang, C. & Kim, W.S. (2015). Recent progress on magnetic iron oxide nanoparticles: synthesis, surface functional strategies and biomedical applications. *Science & Technology of Advanced Materials*, 16(2), 023501.

Yuan, M., Bancroft, E. A., Chen, J., Srinivasan, R. & Wang, Y. (2022). Magnetic fields and magnetically stimulated gold-coated superparamagnetic iron oxide nanoparticles differentially modulate L-type voltage-gated calcium channel activity in midbrain neurons. *ACS Applied Nano Materials*, 5 (1), 205-215. DOI: 10.1021/acsanm.1c02665